Spectrochimica Acta Part A: Molecular and Biomolecular Spectroscopy 211 (2019) 114–124

Contents lists available at ScienceDirect

Spectrochimica Acta Part A: Molecular and Biomolecular Spectroscopy

journal homepage: www.elsevier.com/locate/saa

Novel A^2-D-A^1-D-A^2 type NIR absorbing symmetrical squaraines based on 2, 3, 3, 8-tetramethyl-3H-pyrrolo [3, 2-h] quinoline: Synthesis, photophysical, electrochemical, thermal properties and photostability study

Sushil Khopkar, Mahesh Jachak, Ganapati Shankarling *

Dyestuff Technology Department, Institute of Chemical Technology, N. P. Marg, Matunga, Mumbai 400019, Maharashtra, India

ARTICLE INFO

Article history:
Received 31 August 2018
Received in revised form 28 November 2018
Accepted 28 November 2018
Available online 30 November 2018

Keywords:
Squaraines
NIR absorbing dyes
Acceptor-donor-acceptor-donor-acceptor
2, 3, 3, 8-tetramethyl -3H-pyrrolo [3, 2-h] quinoline
Red shift
DFT computations

ABSTRACT

Two novel acceptor–donor-acceptor-donor-acceptor (A^2-D-A^1-D-A^2) type pi-conjugated symmetrical squaraine dyes, denoted by **PQSQ 1** and **PQSQ 2** based on 2, 3, 3, 8-tetramethyl -3H-pyrrolo [3,2-h] quinoline were successfully synthesized for the first time to arrive absorption and emission at NIR region. These dyes comprise indolenines as electron donor units, squaryl ring as a central electron acceptor and pyridines as terminal electron acceptor units. The relationship between molecular structures and photophysical properties of these dyes was studied in comparison with their parent compounds (**ISQ** and **N-Et ISQ**). These novel squaraine dyes displayed an intense absorption within the range 671 to 692 nm in polar to non- polar solvents respectively with good molar extinction coefficients ($\sim 10^5$ $Lmol^{-1}$ cm^{-1}). Compared to their parent squaraines, both dyes showed red-shifted absorption (33–44 nm) as well as emission (38–59 nm) due to the electron-accepting ability of the ancillary pyridine acceptors and extended pi-conjugation. These dyes exhibited negative solvatochromism and Reichardt's ET (30) scale was applied to propose a quantitative relationship of the relative stability of ground and excited-state of these squaraines with solvent polarity. The electrochemical and computational properties of these symmetrical squaraines were investigated with the help of cyclic voltammetry and density functional theory (DFT). Moreover, **PQSQ 1–2** exhibited high thermal and photo-stability. These A^2-D-A^1-D-A^2 type dyes showed improved photostabilities compared to their parent D-A-D type dyes.

1. Introduction

Symmetrical squaraine dyes are donor-acceptor-donor (D-A-D) type pi-conjugated compounds which are well known for their unique properties such as an intense absorption-emission in the NIR region, intramolecular charge transfer (ICT), high molar extinction coefficients, zwitter-ionic and planar conjugated structure, high redox reversibility, good singlet oxygen generation ability and photostability [1–4]. Owing to these favorable properties, these dyes have attracted high technological applications such as sensitizers in dye-sensitized solar cells, photosensitizers in photodynamic therapy, electrophotography, chemosensors and fluorescent probes [5–9]. The absorption and emission properties of squaraines mainly depend on electron donor strength of terminal aromatic or heterocyclic moieties and linear extension of cyclobutene core. A lot of research has been done in order to shift absorption of squaraines at longer wavelength such as use of pi-extended heterocycles at 1, 3-position of cyclobutene ring [10], substitution of oxygen of squaryl ring by sulphur (synthesis of thiosquaraines) [11], functionalization of squaraine core with electron withdrawing group (synthesis of core substituted squaraines) [12], synthesis of aza- substituted squaraines [13], synthesis of dianionic squaraines [14], synthesis of bridging squaraines [15] and introduction of an electron withdrawing group such as nitro group on donor moiety [16] (Fig. 1). To arrive at NIR absorption - fluorescence properties and various applications, indolenine based squaraines can be modified at (i) N- alkyl group of indolenine moiety (position 1) (ii) squaryl moiety (iii) position 4,5,6,7 of indolenine moiety. Here, we are interested in understanding the role of terminal pyridine acceptors on main donor-acceptor-donor (D-A-D) core (modification at 6 and 7 positions of indolenine) in altering the photophysical properties of novel symmetrical squaraines.

In recent years, various synthetic approaches have been attempted to tune the electrical and optical properties, HOMO-LUMO energy levels of conjugated molecules. One of the most effective approach to influence the HOMO and LUMO energy levels involves incorporation of additional acceptors on main donor-acceptor-donor backbone i.e. acceptor-donor-acceptor-donor-acceptor (A^2-D-A^1-D-A^2) system also referred as a *pull-push-pull-push-pull* system which can depress excited state energy by enhancement of an intramolecular charge transfer [17,18]. Their notable properties are tunable optical and electrical properties, low band gaps resulting in red-shifted absorption-emission spectra and good intramolecular charge transfer [19,20]. Indolenine, a unique and widely accepted

* Corresponding author.
E-mail address: gsshankarling@gmail.com (G. Shankarling).

https://doi.org/10.1016/j.saa.2018.11.061
1386-1425/

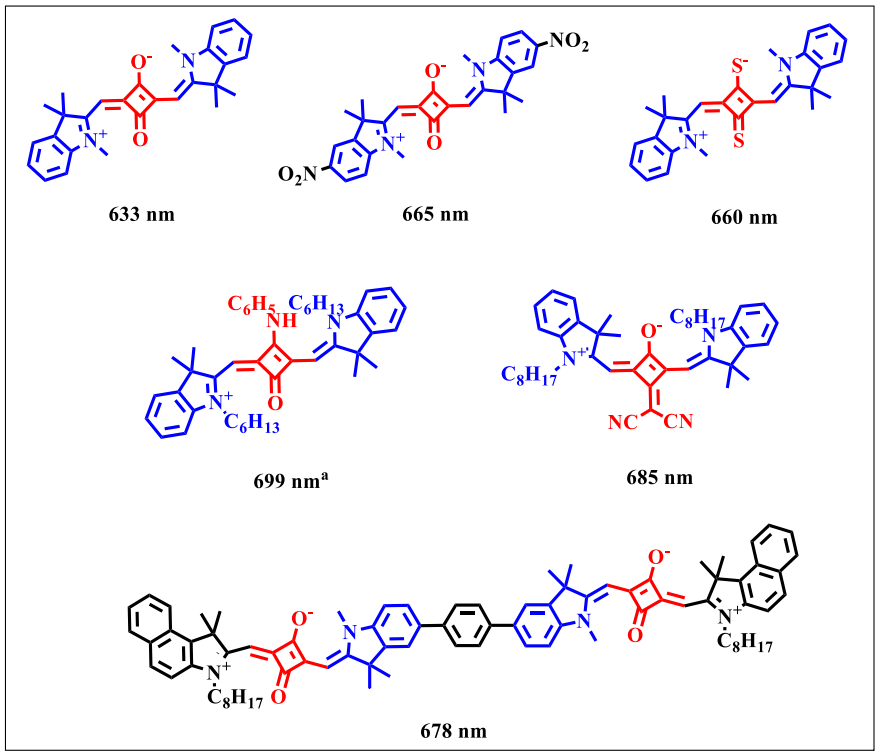

Fig. 1. Reported indolenine based symmetrical squaraines with λ_{max} in chloroform. [a]Absorption maxima measured in MeOH: CH_2Cl_2 (99:1).

electron donor heterocyclic moiety due to its electron-rich nitrogen, has been applied in squaraine chemistry for synthesis of symmetrical squaraines [21], semisquaraines [22], unsymmetrical squaraines [23], pi-extended squaraines [24], bis-squaraines [25], thio-squaraines [26] and acceptor substituted squaraines [27]. Pyridine represents widely used electron accepting unit which contributes to conjugation of the backbone system as well as shifts HOMO-LUMO levels of D-A, D-A-D, A-D-A and A-D-A-D-A type conjugated molecules due to its large electron affinity and intramolecular charge transfer properties. Introduction of a pyridine group on donor-acceptor conjugated system leads to a significantly reduced HOMO-LUMO energy gap and red-shifted absorption [28,29]. Karpagam et al. synthesized donor-acceptor type conjugated molecules consisting pyridine as terminal acceptor units [30].

With these perspectives, here we present synthesis and characterization of two novel A^2-D-A^1-D-A^2 type symmetrical squaraines based on 2, 3, 3, 8-tetramethyl-pyrrolo [3, 2-h] quinoline denoted as, **PQSQ 1** and **PQSQ 2** (Fig. 2). Our main goal is to examine the structure-property relationship of these squaraines to gain a clear understanding of how ancillary terminal acceptor units influences the photophysical properties of conjugated D-A-D backbone. It is hoped that these type of squaraines would result in enhancement of absorption band to NIR region due to the presence of extra terminal acceptor groups and larger pi-conjugated system compared to its parent symmetrical squaraines. The solvatochromic, electrochemical, thermal and photostability properties of synthesized squaraines were also investigated. To the best of our knowledge, there has been no research on such type of A^2-D-A^1-D-A^2 type squaraines.

2. Experimental

2.1. Chemicals and Instruments

All chemicals and reagents were of analytical grade, most of which were procured from SD Fine Chemical Ltd. and some from Finar Ltd. and were used without further purification. ^1H (500 MHz) and ^{13}C (101 MHz) NMR spectra were recorded on Agilent instrument with $CDCl_3$ as a solvent and TMS as an internal standard. ESI-MS analyses were performed on Agilent 6550 mass spectrometer. FT- IR spectra were recorded on Bruker alpha spectrometer using KBr pellets. UV–Visible spectra measurements were performed with a Perkine Elmer Lambda-25 spectrophotometer at room temperature. Fluorescence spectra measurements were performed with a Varian Cary Eclipse fluorescence spectrofluorometer at room temperature.

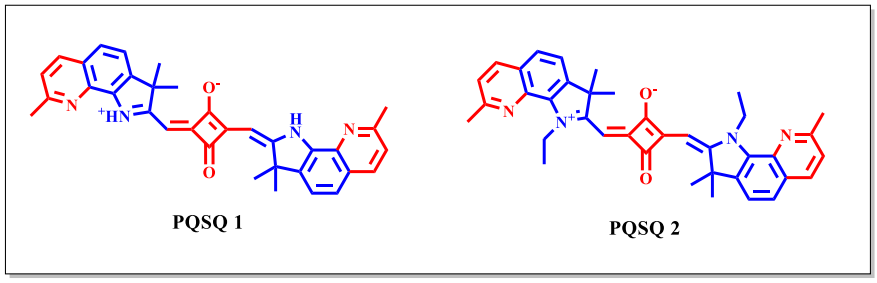

Fig. 2. Molecular structures of newly synthesized squaraines.

2.2. Synthesis

2.2.1. 8-Hydrazinyl-2-Methyl Quinoline Hydrochloride (2)

8-hydrazinyl-2-methyl quinoline hydrochloride **2** was synthesized according to the reported method by diazotization of 8-amino quinaldine **1** followed by reduction using stannous chloride [31].

2.2.2. 2, 3, 3, 8-Tetramethyl-3H-Pyrrolo[3, 2-h]Quinoline (3)

In 50 ml of 4 M aq. HCl, 8-hydrazinyl-2-methyl quinoline hydrochloride **2** (2.0 g, 9.5 mmol) and 3-methyl-butan-2-one (1.0 g, 11.4 mmol) were added. The reaction mass was then heated at 100 °C for next 5 h. After completion of the reaction, the reaction mass was cooled to room temperature and extracted with 100 ml of diethyl ether. Further, the aqueous layer was neutralized with 1 M aq. NaOH and extracted with ethyl acetate. The ethyl acetate layer was separated and evaporated under reduced pressure to give the crude product. The crude product was then purified by column chromatography (eluent system: n- hexane-ethyl acetate, 6:4) to afford pale yellow solid **3** (1.17 g, 55%).

2.2.3. 1-Ethyl-2, 3, 3, 8-Tetramethyl-3H-Pyrrolo [3, 2-h] Quinolin-1-Ium Iodide (5)

To a solution of 2, 3, 3, 8-tetramethyl-3Hpyrrolo [3, 2-h] quinoline **3** (0.6 g, 2.6 mmol) in 20 ml dichloromethane, ethyl iodide (0.43 ml, 5.3 mmol) was added slowly under stirring. The reaction mixture was heated to reflux for 10 h. The reaction mass was then cooled to room temperature and the solvent was evaporated under vacuum. The crude product obtained was washed with methanol to give purified product **5** (0.54 g, 54%).

2.2.4. (Z)-3-Oxo-2-((Z)-(3,3,8-Trimethyl-1,3-Dihydro-2H-Pyrrolo[3,2-h] Quinolin-2-ylidene)Methyl)-4-((3,3,8-Trimethyl-3H-Pyrrolo[3,2-h] Quinolin-1-Ium-2 Yl)Methylene)Cyclobut-1-en-1-Olate (PQSQ 1)

To the azeotropic mixture of n-BuOH: toluene (20 ml 1:1 v/v) were added 2, 3, 3, 8-tetramethyl-3H-pyrrolo [3, 2-h] quinoline **3** (0.5 g, 2.2 mmol), 3, 4-dihydroxy-3-cyclobuten-1, 2-dione **4** (0.127 g, 1.1 mmol) and quinoline (1 ml). The mixture was then refluxed for 6 h. After completion of the reaction, the solvent was removed under vacuo. The crude product obtained was purified by column chromatography (eluent system: dichloromethane: methanol, 9:1) to give green coloured solid (0.8 g, 68%).

2.2.5. (Z)-2-((Z)-(1-Ethyl-3,3,8-Trimethyl-1,3-Dihydro-2H-Pyrrolo[3,2-h] Quinolin-2-ylidene)Methyl)-4-((1-Ethyl-3,3,8-Trimethyl-3H-Pyrrolo[3,2-h] Quinolin-1-Ium-2-Yl)Methylene)-3-Oxocyclobut-1-en-1-Olate (PQSQ 2)

To the azeotropic mixture of n-BuOH: toluene (20 ml 1:1 v/v) were added 1-ethyl 2, 3, 3, 8-tetramethyl-3H-pyrrolo [3, 2-h] quinoline **5** (0.5 g, 1.3 mmol), 3, 4-dihydroxy-3-cyclobuten-1, 2-dione **4** (0.074 g, 0.6 mmol) and quinoline (1 ml). The mixture was then refluxed for 6 h.After completion of reaction solvent was removed under vacuo. The crude product obtained was purified by column chromatography (eluent system: dichloromethane: methanol, 9:1) to give green coloured solid (0.5 g, 65%).

2.3. Compounds Characterization

2.3.1. 2, 3, 3, 8-Tetramethyl-3H-Pyrrolo [3, 2-h] Quinoline (3)

Pale yellow coloured solid,Yield: 55%, M.P: 140 °C, ^{1}H NMR (500 MHz, $CDCl_3$, TMS): δ 8.04 (d, J = 8.4 Hz, 1H), 7.63 (d, J = 8.0 Hz, 1H), 7.42 (d, J = 8.0 Hz, 1H), 7.26 (d, J = 7.1 Hz, 1H), 2.82 (s, 3H), 2.40 (s, 3H), 1.35 (s, 6H).

2.3.2. (Z)-3-Oxo-2-((Z)-(3,3,8-Trimethyl-1,3-Dihydro-2H-Pyrrolo[3,2-h] Quinolin-2-ylidene)Methyl)-4-((3,3,8-Trimethyl-3H-Pyrrolo[3,2-h] Quinolin-1-Ium-2 Yl)Methylene)Cyclobut-1-en-1-Olate (PQSQ 1)

Green coloured solid, Yield: 68%, M.P: 338 °C, ^{1}H NMR (500 MHz, $CDCl_3$, TMS): δ 8.03 (d, J = 8.5 Hz, 2H), 7.49 (d, J = 8.1 Hz, 2H), 7.38 (d, J = 8.1 Hz, 2H), 7.30 (d, J = 8.5 Hz, 2H), 5.68 (s, 2H), 2.82 (s, 6H), 1.53 (s, 12H). ^{13}C NMR (101 MHz, $CDCl_3$): δ 183.62, 175.16, 159.42, 140.28, 138.24, 137.53, 135.91, 135.39, 128.50, 126.69, 122.44, 122.19, 119.49, 86.98, 50.13, 26.46, 25.53. FT-IR (KBr, cm^{-1}): 3424,2965,2925, 1602,1565,1530,1476.1461,1385,1366,1333,1289,1269,1243,1220, 1174,1159,1086,1059,1031,985,921,898,898,841. ESI-MS: m/z calcd for $C_{34}H_{30}N_4O_2$ (M^+): 526.2369, found: 527.2662 (M + 1).

2.3.3.

Green coloured solid, Yield: 65%, M.P:294 °C, ^{1}H NMR (500 MHz, $CDCl_3$,TMS): δ 8.03 (d, J = 8.5 Hz, 2H), 7.52 (d, J = 8.1 Hz, 2H), 7.46 (d, J = 8.0 Hz, 2H), 7.25 (d, J = 10.0 Hz, 2H), 6.15 (s, 2H), 5.20–5.06 (m, 4H), 1.83 (s, 12H), 1.53 (d, J = 6.8 Hz, 6H). ^{13}C NMR (101 MHz, $CDCl_3$): δ 183.62, 178.14, 174.09, 171.32, 159.26, 158.08, 142.97, 138.31, 137.59, 136.61, 126.73, 122.40, 119.50, 86.63, 49.85, 41.70, 26.62, 25.56, 13.61. FT-IR (KBr, cm^{-1}): 3439, 2962, 2922, 2853, 1593, 1565, 1527, 1485, 1453, 1414, 1383, 1333, 1265, 1235, 1190, 1105, 1086, 1061, 1011, 897, 840, 794. ESI-MS: m/z calcd for $C_{38}H_{38}N_4O_2$ (M^+): 582.2995, found: 582.3230.

3. Results and Discussion

3.1. Synthetic Strategy

To check out the influence of ancillary pyridyl acceptor groups on main donor-acceptor-donor (D-A-D) backbone of squaraine, two different A^2-D-A^1-D-A^2 type squaraine dyes **PQSQ 1** and **PQSQ 2** were successfully synthesized. Scheme 1 displays the synthetic protocol used to prepare these dyes. The key intermediate 2, 3, 3, 8-tetramethyl-3H-pyrrolo [3, 2-h] quinoline (**3**) was synthesized by diazotization – reduction of 8-amino −2-methyl quinoline (**1**) followed by Fischer indole synthesis. Two equivalents of 2, 3, 3, 8-tetramethyl-3H-pyrrolo [3,2-h] quinoline intermediate (**3, 5**) allowed to refluxed with one equivalent of squaric acid **4** in n-BuOH: Toluene (1:1 V/V) azeotropic system to afford green coloured products,**PQSQ 1** and **PQSQ 2** with yield of 68% and 65% respectively. The structures of both compounds were confirmed by means of standard spectroscopic techniques (see the Supplementary Information). In order to assess the influence of additional pyridine moieties, two reference symmetrical squaraines **ISQ** and **N-Et ISQ** were synthesized according to reported procedures [32]. ^{1}H NMR spectra of **PQSQ 1** and **PQSQ 2** dyes showed a singlet signal at 5.68 ppm and 6.15 ppm respectively corresponds to characteristic alkenylic protons of symmetrical squaraines (Figs. S2–3). The FT-IR spectra of **PQSQ 1** and **PQSQ 2** dyes showed no C═O stretching at 1600 cm^{-1}. Instead, the characteristic frequencies at 1602 cm^{-1} and 1593 cm^{-1} were observed corresponding to C═C stretching in the four-membered ring (Figs. S8–9). These dyes contained an electron donating indolenine moiety and electron withdrawing pyridine and squaryl moieties as a terminal and central acceptors linked through pi-bridge. The synthesized squaraines were modified at N-alkyl (ethyl) group of indolenine to check the effect of alkyl groups on photophysical properties of squaraines. It is predictable that such kind of A^2-D-A^1-D-A^2 system will provide a large conjugated system and strong intramolecular charge transfer characteristics resulting in red-shifted absorption and emission relative to their parent D-A-D type squaraines.

3.2. Photophysical Properties

As different solvents can change the energy levels of ground state as well as an excited state of molecules and consequently, change the absorption and emission bands, we have studied the primary photophysical properties of **PQSQ 1–2** dyes in eight different solvents of different dielectric constants and refractive indices. Fig. 3 represents the absorption and emission spectra of these dyes at concentration of 5×10^{-6} M. Table 1 shows the relevant photophysical data such as absorption maxima (λ_{max}), molar extinction coefficient (ε), optical band gap (ΔE_{opt}), emission

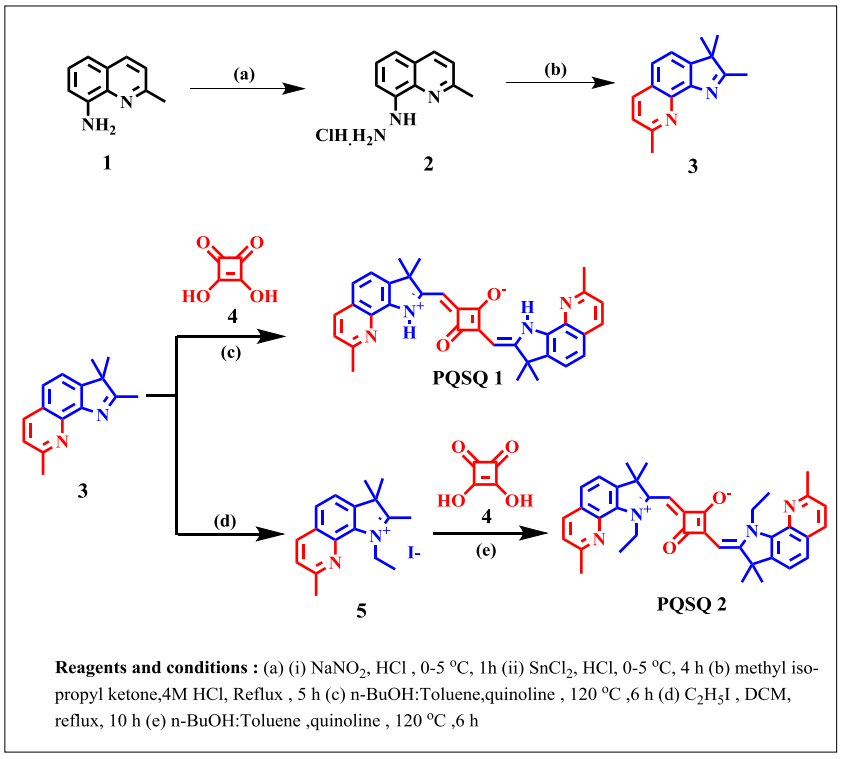

Scheme 1. Synthesis of symmetrical squaraines.

maxima (λ_{em}), Stokes shift (λ_s), fluorescence quantum yield (ϕ) and oscillator strength (f) of these dyes in different solvents. These novel squaraine dyes displayed an intense absorption within NIR range of 671–692 nm and emission in the range 691–718 nm which can be assigned to an intramolecular charge transfer transition of a large conjugated molecule. The UV–Visible spectra of **PQSQ 1** exhibited a strong absorption band at 687 nm in chloroform. Under similar conditions, **PQSQ 2** showed absorption at 678 nm which is blue shifted in comparison to **PQSQ 1**. A similar trend was observed in emission spectra of these dyes. In addition, these compounds showed blue shifted absorption with increasing solvent polarity (negative solvatochromism). For example, in non-polar solvent toluene, **PQSQ 1** and **PQSQ 2** showed absorption maxima at 694 nm and 686 nm respectively. When solvent polarity was increased, absorption maxima were blue shifted to 679 and 671 nm in methanol. The molar extinction coefficients of these novel dyes were very high ($>10^5$ $Lmol^{-1}$ cm^{-1}). The full width at half maximum (FWHM) values for these compounds were in between 39 and 49 nm. Moreover, **PQSQ 1** exhibited low optical band gap (ΔE_{opt}) than **PQSQ 2**. For example, **PQSQ 1** showed ΔE_{opt} at 1.73 eV in methanol. In the case of **PQSQ 2**, it increased to 1.76 eV. Stokes shift values for these dyes ranged from 24 to 59 nm and **PQSQ 1** exhibited the red shift compared to **PQSQ 2** in all studied solvents. The fluorescence quantum yields of these dyes were determined by using methylene blue as a standard ($\phi_s = 0.52$ in chloroform) [33] and calculated using eq. (I)

$$\phi_u = \frac{\phi_s . \ A_s \ . F_u . n_u^2}{A_u . F_s . n_s^2} \quad \text{(I)}$$

where ϕ_u and ϕ_s are the quantum yield of unknown and standard, A_u and A_s are the absorbance of unknown and standard, F_u and F_s are the integrated fluorescence intensity at the excitation wavelength of unknown and standard, n_u and n_s are the refractive indexes of the solvent of unknown and standard respectively. The **PQSQ 1** and **PQSQ 2** dyes gave the highest fluorescence quantum yield of 0.64 and 0.60 respectively in chloroform.

From the available absorption data of these dyes, we calculated its oscillator strengths (f) using well known expression [34].Due to the large molar extinction coefficients, higher values (0.68–1.05) of oscillator strengths (f) were observed for these dyes demonstrating good charge transfer characteristics and the ability of these squaraines to collect light.

From Fig. 3A and B, it is observed that both dyes **PQSQ 1** and **PQSQ 2** exhibited blue-sided vibronic shoulder peaks with red-sided main absorption peaks in all studied solvents. The shoulder peak is may be due to the formation of H-aggregates in concentrated solution which absorbs in that region [35]. The H-aggregates formation was then confirmed from the absorption spectra of **PQSQ 1** and **PQSQ 2** with different concentrations in chloroform (Fig. 4). At concentrated solutions (5×10^{-6} M), **PQSQ 1** and **PQSQ 2** showed main absorption peaks at 687 nm and 678 nm with shoulder peaks at 630 nm and 623 nm respectively. Upon dilution of solution from 5×10^{-6} M to 5×10^{-8} M, the shoulder peaks get disappeared which gives strong evidence that shoulder peaks of **PQSQ 1** and **PQSQ 2** are results of H-aggregates formation.

The absorption maxima of indolenine based symmetrical squarylium dyes was bathochromically shifted by the introduction of an electron acceptor on indolenine donor [36]. Here, we studied the effect of ancillary pyridine moieties which acts as acceptors and extends the pi-conjugation of the A^2-D-A^1-D-A^2 system on its photophysical properties. For this purpose, we compared the photophysical properties of our novel squaraines (**PQSQ 1** and **PQSQ 2**) and corresponding parent squaraines (**ISQ** and **N-Et ISQ**). The **ISQ** and **N-Et ISQ** dyes have D-A-D design consisting of squaryl acceptor flanked by two terminal indolenine donors whereas **PQSQ 1** and **PQSQ 2** are A^2-D-A^1-D-A^2 type dyes having pyridine, indolenine, and squaryl ring as a terminal acceptors, donors, and central acceptor respectively. Fig. 5 represents the normalized absorption and emission spectra of these dyes in chloroform. Table 2 displays absorption maxima, emission maxima, Stokes shift and the optical band gap of these dyes in chloroform. Interestingly, the red-shifted absorption and emission, as well as large Stokes shifts, were observed when pyridine moiety introduced into D-A-D core of squaraines. The absorption maxima (λ_{max}) of **PQSQ 1** showed a red

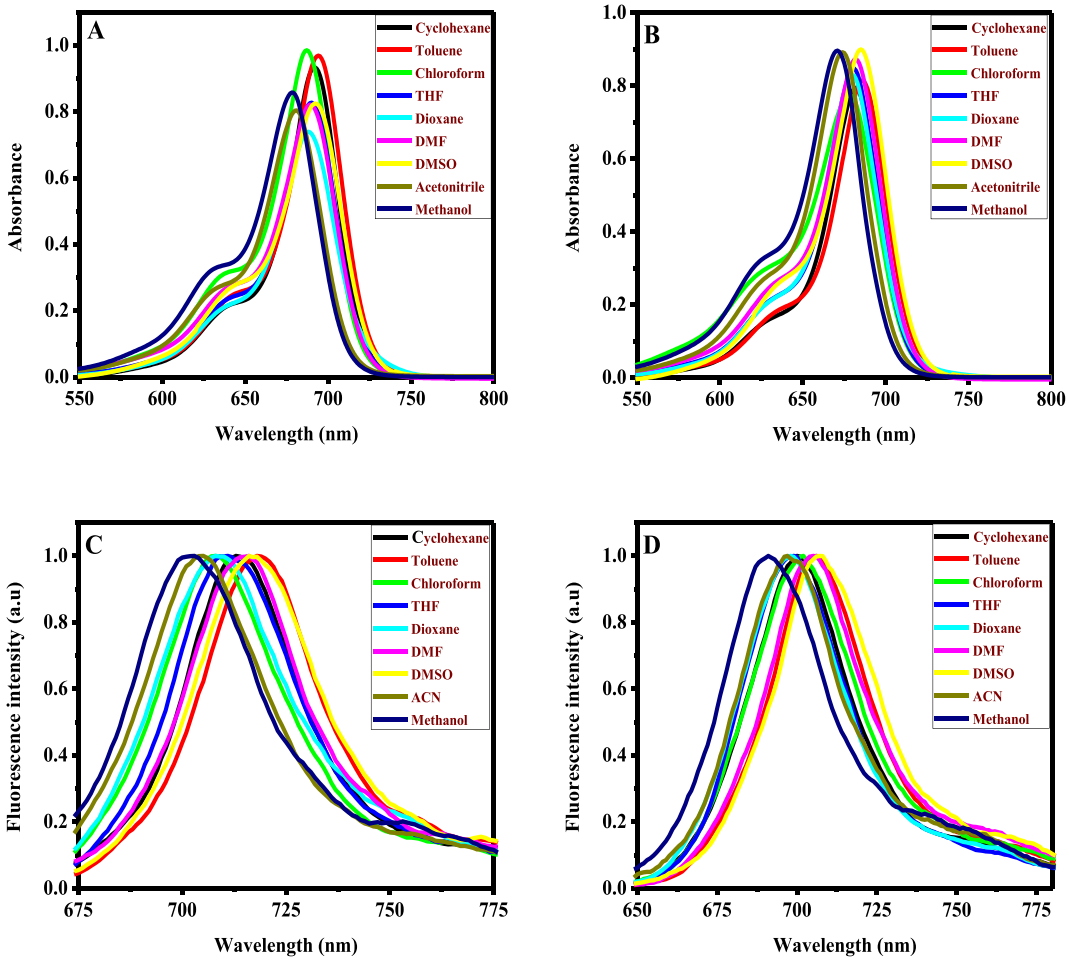

Fig. 3. (A) Absorption spectra of **PQSQ 1** (B) Absorption spectra of **PQSQ 2** (C) Normalized emission spectra of **PQSQ 1** (D) Normalized emission spectra of **PQSQ 2** in different solvents at concentration 5×10^{-6} M.

Table 1
Photophysical data of **PQSQ 1** and **PQSQ 2** in different solvents.

Compound	Solvent	λ_{max}[a] (nm)	Log ε[b]	FWHM[c]	λ_{onset}[d]	ΔE_{opt}[e] eV	λ_{em}[f] (nm)	λ_s[g] (nm)	ϕ[h]	f[i]
PQSQ 1	Cyclohexane	692	5.27	36.1	732.35	1.69	713	21	0.31	0.71
	Toluene	694	5.29	37.6	726.58	1.71	718	24	0.34	0.75
	Chloroform	687	5.29	39.3	728.02	1.70	708	21	0.64	0.96
	THF	690	5.22	39.4	730.91	1.70	711	21	0.37	0.74
	1,4-dioxane	688	5.17	41.7	729.47	1.70	708	20	0.21	0.68
	DMF	689	5.22	41.2	728.02	1.70	716	27	0.38	0.82
	DMSO	692	5.22	42.7	732.35	1.69	717	25	0.43	0.73
	Acetonitrile	681	5.21	41.3	720.91	1.72	705	24	0.38	0.88
	Methanol	679	5.23	42.0	715.14	1.73	703	24	0.31	0.99
PQSQ 2	Cyclohexane	682	5.20	36.6	716.59	1.73	700	18	0.28	0.69
	Toluene	686	5.21	36.8	722.36	1.72	706	20	0.31	0.70
	Chloroform	678	5.19	48.0	720.92	1.72	702	24	0.60	1.00
	THF	681	5.23	37.8	719.47	1.72	699	18	0.32	0.81
	1,4-dioxane	680	5.22	38.6	720.92	1.72	698	18	0.14	0.80
	DMF	682	5.24	40.2	718.02	1.73	705	23	0.34	0.90
	DMSO	685	5.26	40.6	723.81	1.71	707	22	0.37	0.82
	Acetonitrile	674	5.25	39.6	715.14	1.73	697	23	0.31	0.96
	Methanol	671	5.25	40.5	705.25	1.76	691	20	0.28	1.05

[a] Absorption maximum at molar concentration 5×10^{-6} M.
[b] Molar extinction coefficient determined from absorbance for molar concentration 5×10^{-6} M.
[c] Full width at half maximum.
[d] Onset absorption edge at a higher wavelength.
[e] Optical band gap, $\Delta E_{opt} = 1240 \times \lambda_{onset}$.
[f] Emission at molar concentration 5×10^{-6} M.
[g] Stokes shift.
[h] Quantum yield calculated using methylene blue as a standard ($\phi = 0.54$ in chloroform).
[i] Oscillator strength.

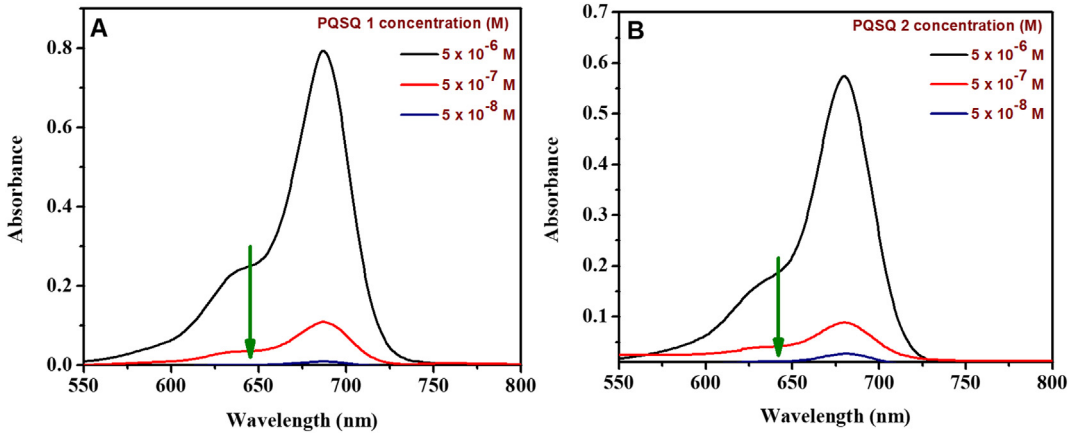

Fig. 4. Absorption spectra of (A) **PQSQ 1** (B) **PQSQ 2** with different concentrations in chloroform.

shift of 33 nm compared to its parent indolenine based squaraine **ISQ**. Similarly, λ_{max} of **PQSQ 2** was red shifted by 44 nm compared to **N-Et ISQ**. A similar trend was also observed in the emission spectra of these squaraines. The emission wavelength of **PQSQ 1** and **PQSQ 2** was bathochromically shifted by 38 nm and 59 nm compared to **ISQ** and **N-Et ISQ** respectively. This bathochromic shift in optical properties of **PQSQ 1–2** can be attributed to an increased pi-conjugation of the A^2-D-A^1-D-A^2 system and effective intramolecular charge transfer between donor and acceptors. Furthermore, the Stokes shift of newly synthesized squaraines **PQSQ 1–2** exhibited a red shift of 5 nm and 15 nm with respect to corresponding reference dyes **ISQ** and **N-Et ISQ** indicating an increased charge transfer characteristics of these novel dyes. Additionally, the optical band gap (ΔE_{opt}) of these squaraines calculated from onset of low energy band (1.72 eV for **PQSQ 1** and 1.73 eV for **PQSQ 2**) was found to be less compared to parent squaraines (1.79 eV for **ISQ** and 1.86 eV for **N-Et ISQ**) indicating larger delocalization and *pull-push-pull-push-pull* effect of these novel dyes. Therefore, from spectral data, it is confirmed that the introduction of additional terminal acceptors in the A^2-D-A^1-D-A^2 system could be favorable for long wavelength absorption and emission with respect to D-A-D system.

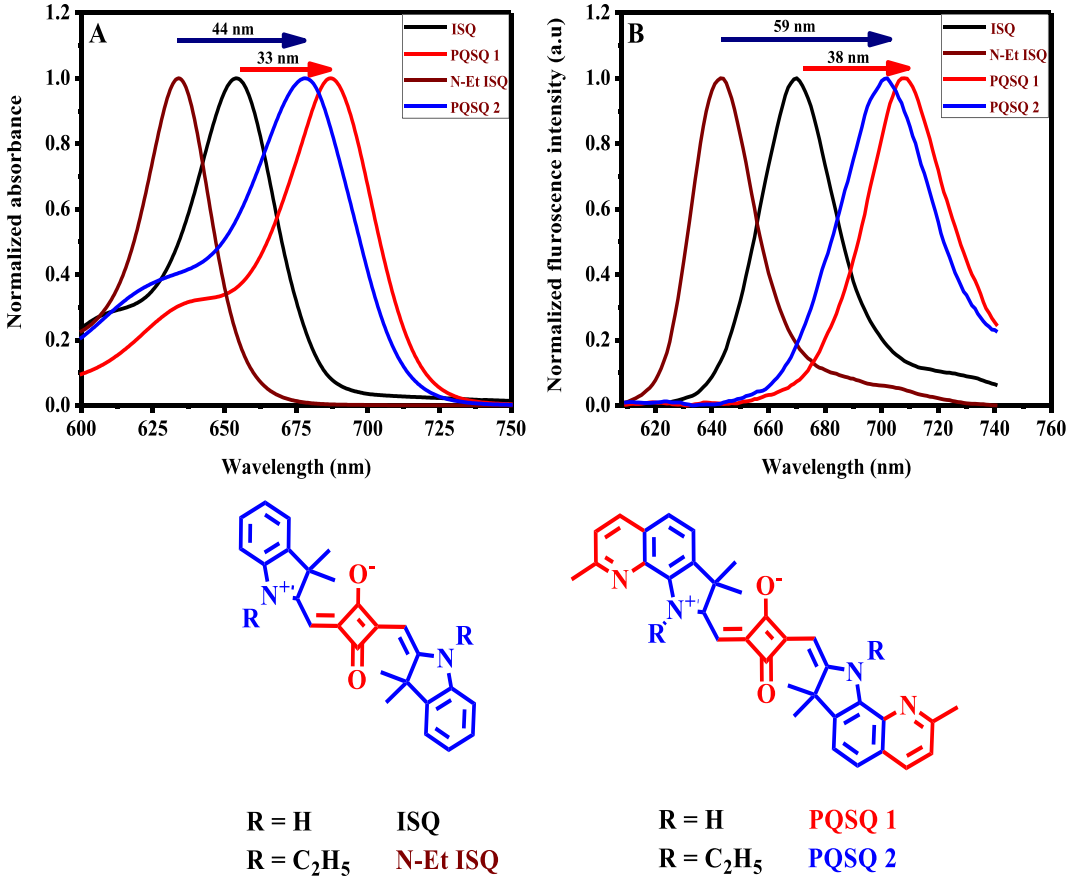

Fig. 5. (A) Normalized absorption spectra (B) Normalized emission spectra of **PQSQ 1**, **PQSQ 2**, **ISQ** and **N-Et ISQ** in chloroform at concentration 5×10^{-6} M.

Table 2
Comparison of photophysical properties of **PQSQ 1**, **PQSQ 2**, **ISQ** and **N-Et ISQ** at concentration 5×10^{-6} M.

Compound	Solvent	λ_{max} [a] (nm)	λ_{em} [b] (nm)	λ_s [c] (nm)	λ_s [c] (cm^{-1})	λ_{onset} [d] nm	ΔE_{opt} [e] eV
ISQ	Chloroform	654	670	16	365.14	693.81	1.79
PQSQ 1	Chloroform	687	708	21	431.75	722.36	1.72
N-Et ISQ	Chloroform	634	643	9	220.77	665.26	1.86
PQSQ 2	Chloroform	678	702	24	504.25	715.45	1.73

[a] Absorption maximum at molar concentration 5×10^{-6} M.
[b] Emission at molar concentration 5×10^{-6} M.
[c] Stokes shift.
[d] Onset absorption edge at a higher wavelength.
[e] Optical band gap, $\Delta E_{opt} = 1240 \times \lambda_{onset}$.

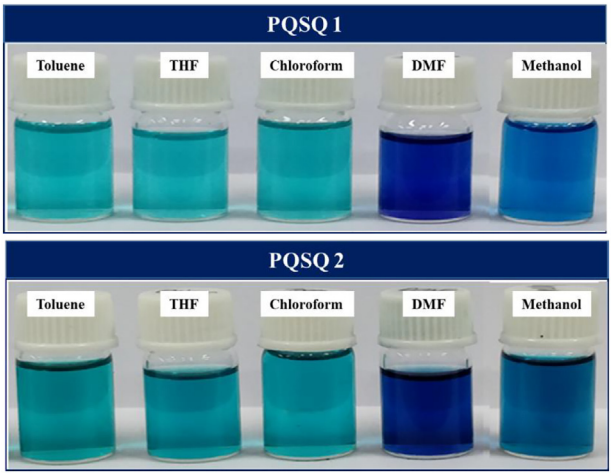

Fig. 6. Negative solvatochromism of **PQSQ 1–2** in various solvents.

3.3. Solvatochromism

From primary photophysical properties, it appeared that in different solvents, **PQSQ 1–2** exhibited different absorption wavelengths (Table 1). The absorption wavelengths showed a blue shift with increasing solvent polarity (negative solvatochromism). For example, in non-polar solvent toluene, absorption maxima of **PQSQ 1** and **PQSQ 2** was observed at 694 nm and 684 nm respectively. As solvent polarity increased, absorption maxima was blue shifted ($\Delta\lambda = 15$ nm for **PQSQ 1**, $\Delta\lambda = 13$ nm for **PQSQ 2**), as demonstrated by a red shift in methanol ($\lambda_{max} = 679$ nm for **PQSQ 1** and 671 nm for **PQSQ 2**). Fig. 6 shows the color changes of **PQSQ 1–2** with increasing polarity of solvents.

To investigate the negative solvatochromic properties of **PQSQ 1** and **PQSQ 2**, UV–Visible absorption spectra in five different solvents of different polarities i.e. toluene, THF, chloroform, DMF and methanol were collected at concentration 5×10^{-6} M and plotted $1/\lambda_{max}$ against ET (30) (Fig. 7). ET (30), empirical solvent polarity scale is a measure of solvent polarity created from intramolecular charge transfer of Reichardt's dye [37]. This solvent polarity scale is used to study the solvatochromic behavior of NIR absorbing cyanine dyes [38]. As the dyes under study are NIR absorbing, having small Stokes shift, we studied the solvatochromic behavior by plotting absorbance versus empirical solvent polarity parameter ET (30). The linear relationship with good regression coefficient (R^2) values (0.86 for **PQSQ 1** and 0.78 for **PQSQ 2**) observed in Fig. 7 confirms the negative solvatochromic properties of these dyes. The observed pronounced negative solvatochromism may be due to an extra stabilization of ground state of these zwitter-ionic dyes compared to excited state as solvent polarity increased. Accordingly, absorption maximum was shifted hypsochromically with an increase in solvent polarity. In other words, apolar solvents stabilize LUMO and destabilize HOMO of **PQSQ 1–2** and consequently, reducing the band gap and opposite occurs in case of polar solvents.

3.4. Electrochemical Properties

To examine the electrochemical properties of **PQSQ 1** and **PQSQ 2**, cyclic voltammograms (CV) have been performed in chloroform using tetrabutylammonium perchlorate (TBAP) as supporting electrolyte, ferrocenium-ferrocene redox couple as an external reference, glassy carbon as a working electrode and Ag/AgCl as a reference electrode with scan rate of 25 mVS^{-1}. For comparison purpose, the cyclic voltammograms of parent dyes **ISQ** and **N-Et ISQ** have also been performed under the same conditions. Fig. 8 displays the overlaid cyclic voltammograms (CV) of newly synthesized squaraines (**PQSQ 1** and **PQSQ 2**) and parent squaraines (**ISQ** and **N-Et ISQ**). Table 3 shows the corresponding CV data of these dyes.

Indolenine based symmetrical squaraines generally show one electron reversible oxidation peak which is attributed to oxidation of an indolenine nitrogen [39]. Consequently, one electron anodic oxidation process of **ISQ** and **N-Et ISQ** in chloroform displayed a good electrochemical reversibility as I_{pa}/I_{pc} ratio of these dyes is almost equal to unity ($I_{pa}/I_{pc} = 0.95$ for **ISQ**, $I_{pa}/I_{pc} = 0.93$ for **N-Et ISQ**) (Fig. 8). However, the electrochemical properties of novel symmetrical squaraines **PQSQ 1–2** differs from the reported indolenine based symmetrical squaraines. The one electron oxidation of **PQSQ 1** and **PQSQ 2** was electrochemically irreversible ($I_{pa} \neq I_{pc}$). Both dyes showed anodic oxidative peak due to oxidation of nitrogen of pyrrolo quinaldine but corresponding cathodic waves were weaker in intensity indicative of the low stability of radical cation [40]. This can be attributed to an introduction of

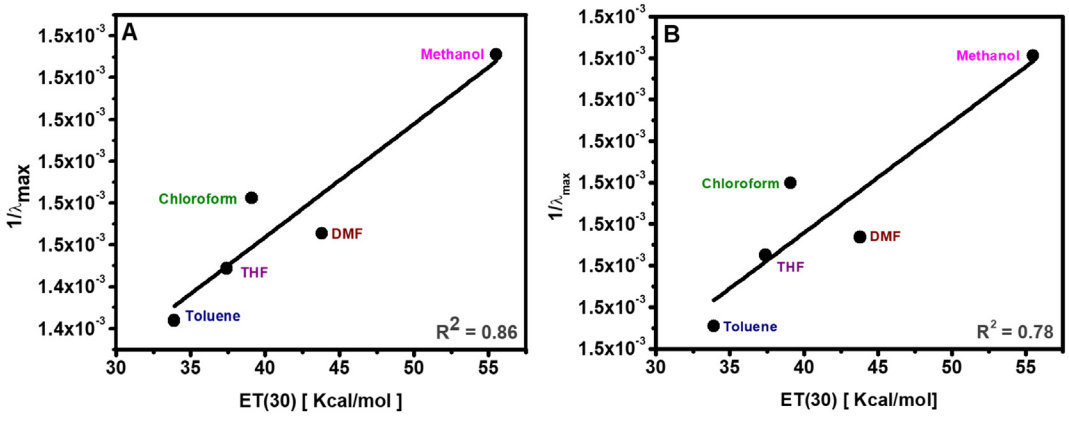

Fig. 7. Plot of $1/\lambda_{max}$ with ET (30) of **PQSQ 1** (A) and **PQSQ 2** (B) in various solvents at concentration 5×10^{-6} M.

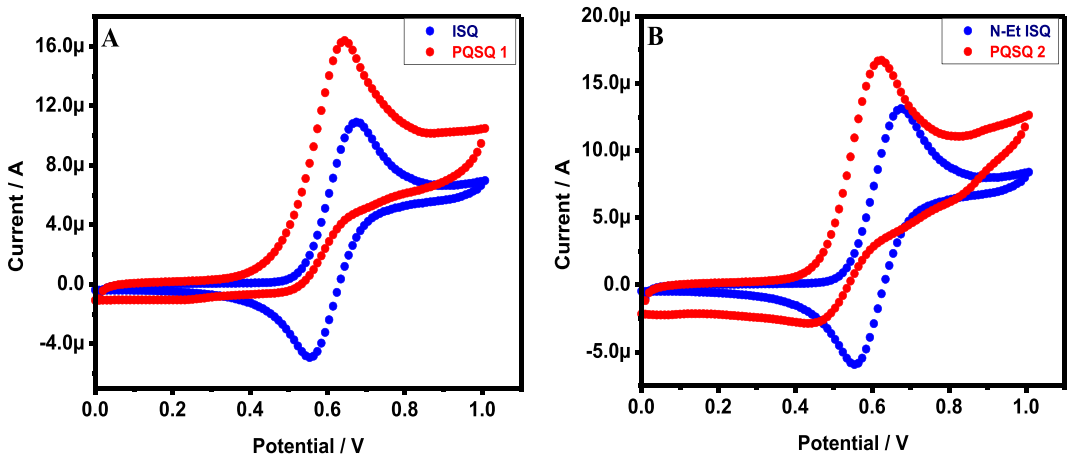

Fig. 8. Overlaid cyclic voltammogram curves of (A) **ISQ** and **PQSQ 1** (B) **N-Et ISQ** and **PQSQ 2** at scan rate 25 mVS^{-1}.

Table 3
Electrochemical and computational data of **ISQ**, **N-Et ISQ**, **PQSQ 1** and **PQSQ 2** in chloroform.

Compound	E_{pa} [a]	E_{pc} [b]	I_{pc}/I_{pa} [c]	Experimental (eV)			Theoretical [g] (eV)		
				E_{HOMO} [d]	E_{LUMO} [e]	Eg [f]	E_{HOMO}	E_{LUMO}	Eg
ISQ	0.69	0.55	0.95	−5.40	−3.61	1.79	−4.84	−2.49	2.35
N-Et ISQ	0.68	0.54	0.93	−5.39	−3.53	1.86	−4.89	−2.53	2.36
PQSQ 1	0.64	–	–	−5.35	−3.64	1.72	−4.72	−2.49	2.23
PQSQ 2	0.62	–	–	−5.33	−3.61	1.73	−4.81	−2.56	2.25

[a] Peak anodic oxidation potential.
[b] Peak cathodic oxidation potential.
[c] I_{pc}/I_{pa} was calculated by Nicholson's equation [41] (see ESI).
[d] $E_{HOMO} = -e\,(E_{ox}\ \text{onset} + 4.71)$ eV.
[e] $E_{LUMO} = E_{HOMO} - E_{o\text{-}o}$, $E_{o\text{-}o}$ = zero-zero excitation energy.
[f] HOMO-LUMO energy gap from CV data.
[g] Density functional theory.

terminal ancillary pyridine acceptors on indolenine moiety of symmetrical squaraines.

The onset value of oxidation potentials for **ISQ** and **N-Et ISQ** were determined to be 0.69 V and 0.68 V, corresponds to HOMO energy levels −5.40 eV for **ISQ** and −5.39 eV for **N-Et ISQ**. Addition of two terminal pyridine moieties to the main D-A-D backbone leads to lowering of the oxidation potential with respect to **ISQ** and **N-Et ISQ**. Thus under same conditions, the **PQSQ 1** and **PQSQ 2** dyes displayed onset oxidation potentials at 0.64 V and 0.62 V, corresponds to HOMO energy levels −5.35 eV and −5.33 eV respectively. The energy of lowest unoccupied molecular orbitals (LUMOs) of these dyes were calculated from the values of E_{ox} and zero-zero excitation energies ($E_{o\text{-}o}$) which is obtained from onset of UV–Visible absorption spectra were found to be −3.61 eV for **ISQ**, −3.53 eV for **N-Et ISQ**, −3.64 eV for **PQSQ 1** and −3.61 eV for **PQSQ 2**. Moreover, enlarging the pi-conjugation of **PQSQ 1–2** resulted in a slight reduction of E_g value. The electrochemical band gap (E_g) values for **PQSQ 1** and **PQSQ 2** were found to be less (1.72 eV for **PQSQ 1** and 1.73 eV for **PQSQ 2**) as compared to its reference squaraines (1.79 for **ISQ** and 1.86 for **N-Et ISQ**). In other words, the introduction of pyridine acceptor on squaraines **PQSQ 1–2** decreases the energy of LUMO and increases the energy of HOMO resulting in reduced HOMO-LUMO band gap compared to its parent squaraines (Fig. 9).

3.5. Computational Properties

For a further understanding of correlation between molecular structures of novel squaraines (**PQSQ 1** and **PQSQ 2**) and its photophysical properties, density functional theory (DFT) was performed using B3LYP [42] functional and def2-TZVP (valence triple–zeta-plus polarization) [43] as a basis set for geometry optimization and calculation of frontier molecular orbital distribution using the Turbomole-V6.5 program [44]. The vertical excitation energies (VEE), oscillator strengths

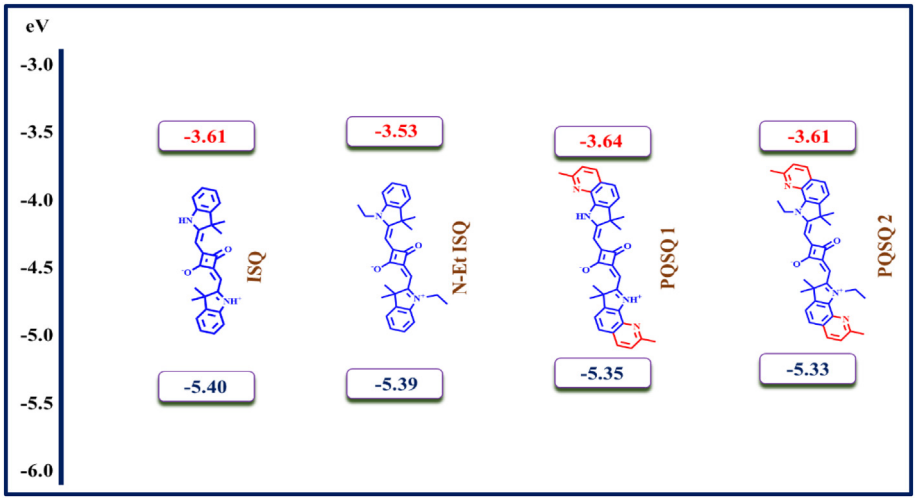

Fig. 9. HOMO-LUMO energy levels of **ISQ**, **N-Et ISQ**, **PQSQ 1** and **PQSQ 2** obtained by cyclic voltammetry.

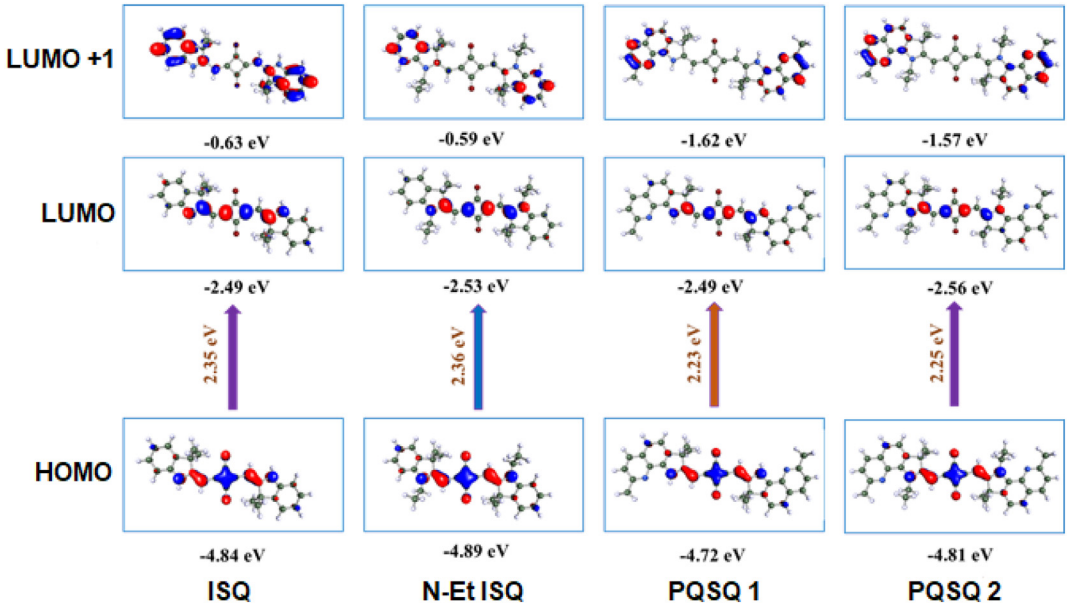

Fig. 10. Frontier molecular orbitals of **ISQ**, **N-Et ISQ**, **PQSQ 1** and **PQSQ 2** optimized at DFT - B3LYP functional and def2-TZVP basis set.

(f) and orbital contributions for lowest 10 singlet transitions in chloroform were elucidated by using time-dependent density functional theory (TD-DFT) with same functional and basis set. For comparison purpose, DFT study of parent dyes **ISQ** and **N-Et ISQ** also carried out using same basis set.

Optimized ground state geometries of all dyes with frontier molecular orbital profiles showing electronic distributions in their HOMO and LUMO levels are displayed in Figs. 10 and Fig. 13. Optimized geometries of these dyes indicated that they have planar conformations. Consequently, the electron density of HOMO and LUMO orbitals spreads over the entire molecule of these dyes. From Fig. 10, it is observed that HOMOs of reference dyes, **ISQ**, and **N-Et ISQ** are situated on indolenine donors and squaryl acceptor. There is a transfer of electron density from the squaryl ring to indolenines at LUMO level while at LUMO+1 the electron density localized only on indolenines. The alkyl groups showed a negligible contribution of electron density suggesting that they have a negligible role in charge transfer mechanism. In the case of **PQSQ 1** and **PQSQ 2** dyes, the HOMOs are predominantly contributed by squaraine core and extended over indolenine. After excitation, electron density from the squaraine core transferred to indolenine. Thus LUMOs of both squaraines can be seen to be equally contributed by squaryl and indolenine moieties. The LUMO +1 of both dyes are contributed mainly by pyridine acceptors with less contribution of indolenine. Ethyl groups have a negligible contribution to molecular orbitals involved in absorption spectra. Thus in an excited state, the electron density shifted from central squaryl acceptor to terminal pyridine acceptors through the pi-framework of indolenine donor which clearly reveals a strong interaction between indolenine donor and acceptors resulting in strong intramolecular charge transfer [45]. Such transfer of electron density from central acceptor to terminal acceptors through donor is absent in **ISQ** and **N-Et ISQ** dyes. In conclusion, the good interaction between donors and acceptors of the A^2-D-A^1-D-A^2 type of dyes leads to the decreased HOMO-LUMO band gap and consequently red-shifted absorption compared to D-A-D type dyes.

Further, to evaluate the computed absorption properties, we compared the HOMO-LUMO energy band gap, vertical excitation energies (VEE), oscillator strengths and orbital configurations of **ISQ** and **N-Et ISQ** dyes with **PQSQ 1** and **PQSQ 2** in chloroform using the TD-DFT method and the results are summarized in Table 4. In general, lower

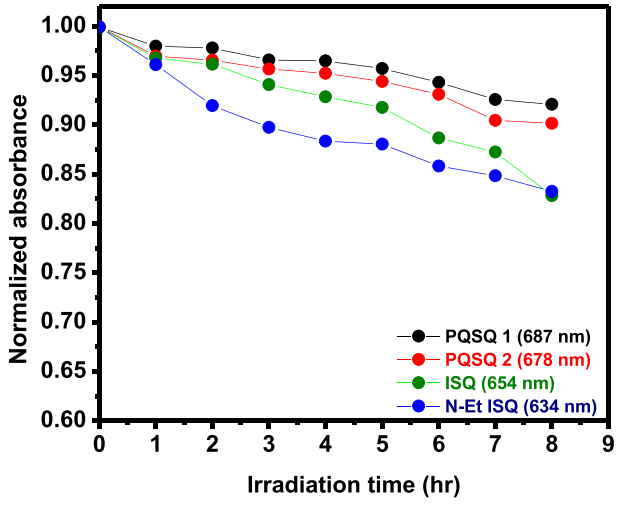

Fig. 11. Change in absorbance of **ISQ**, **N-Et ISQ**, **PQSQ 1** and **PQSQ 2** at maximum absorption wavelength with the irradiation time.

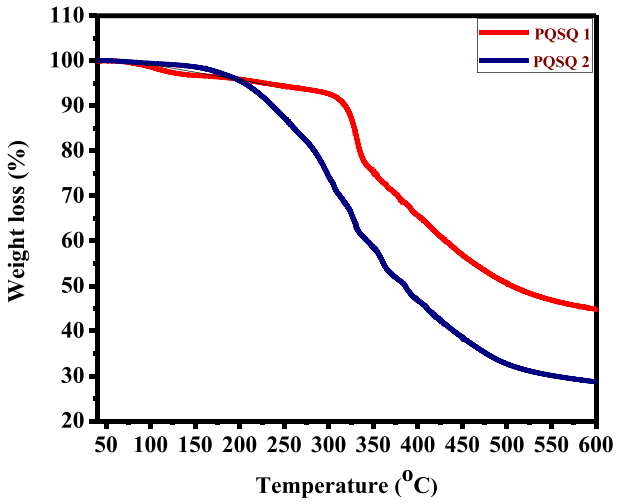

Fig. 12. Thermostability study of **PQSQ 1** and **PQSQ 2**.

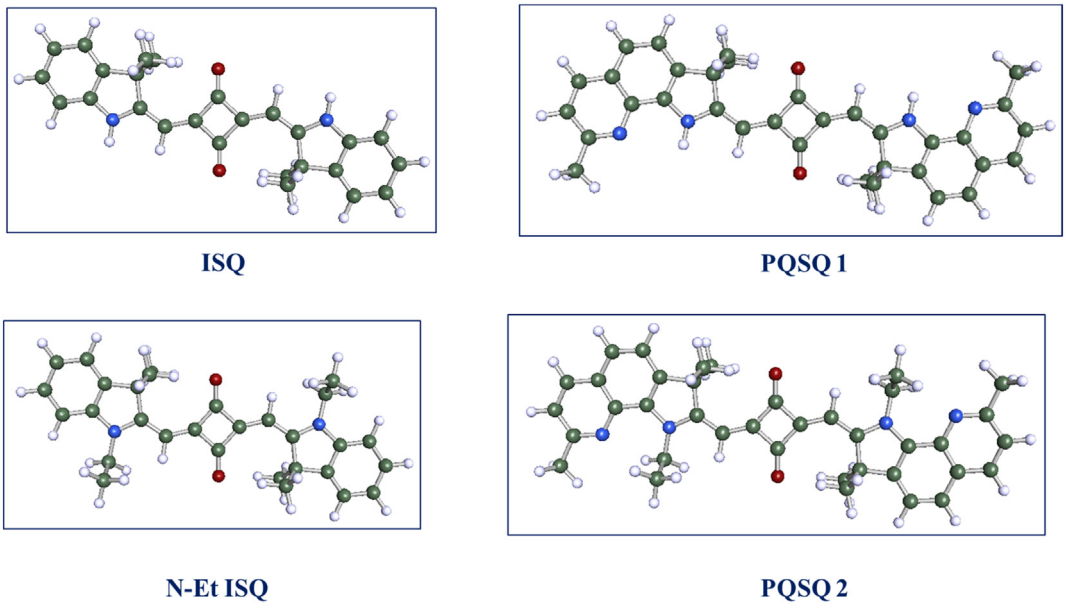

Fig. 13. Optimized geometries of **ISQ**, **N-Et ISQ**, **PQSQ 1** and **PQSQ 2.**

HOMO-LUMO energy gaps were observed for **PQSQ 1** and **PQSQ 2** (2.23 eV for **PQSQ 1**, 2.25 eV for **PQSQ 2**) as compared to **ISQ** and **N-Et ISQ** (2.35 eV for **ISQ**, 2.36 eV for **N-Et ISQ**) due to its large pi-conjugated system (Fig. 14). The computed HOMO-LUMO energy gaps of all dyes displayed similar trends with experimentally determined HOMO-LUMO band gaps obtained from cyclic voltammetry (Table 3). Moreover, the computed vertical excitation of **PQSQ 1** showed a 40 nm red shift compared to **ISQ**. Similarly, **PQSQ 2** showed 39 nm red shift with respect to **N-Et ISQ**. The major contribution of electronic transitions (97–99%) for all dyes is from HOMO to LUMO transition at high oscillator strength. These transitions move the electron density of π-π* framework from squaraine core to pyridine acceptors (intramolecular charge transfer). In addition, the computed oscillator strengths of these novel dyes (1.93 for **PQSQ 1**, 1.94 for **PQSQ 2**) are higher as compared to corresponding parent dyes (1.74 for **ISQ**, 1.74 for **N-Et ISQ**) indicating increased intramolecular charge transfer characteristics of these dyes [46].

3.6. Photostability

A common challenge with various NIR absorbing materials is low photostability during continued irradiation in presence of oxygen which limits their applicability for practical applications such as fluorescence microscopy, photonic and optoelectronic devices. To investigate the relationship between molecular structures and photostabilities of novel squaraines **PQSQ 1–2**, the photostability experiments were performed using 500 W iodine-tungsten (I/W) lamp (working wavelength range = 320–1100 nm). In order to cut off the light shorter than 400 nm, the light of I/W lamp was filtered through the light filter and then irradiated on the samples in chloroform for 8 h at room temperature [47]. The distance between the samples and lamp was 30 cm. For comparison purpose, the photostabilities of two reference dyes, **ISQ**, and **N-Et ISQ** were also investigated under the same conditions and results are shown in Fig. 11.

Fig. 11 reveals that the maximum absorption intensity of **ISQ** and **N-Et ISQ** were decreased by 18.55% and 19.65% respectively to its original value after 8 h irradiation in chloroform solution under nitrogen atmosphere. Under similar conditions, **PQSQ 1** and **PQSQ 2** showed 11.71% and 14.39% decrease in absorption intensity at maximum absorption wavelength. The N-alkyl groups influenced a small contribution to photostabilities of these dyes. The photostability of all studied dyes in order from most stable to least is **PQSQ 1** > **PQSQ 2** > **ISQ** > **N-Et ISQ** after 8 h of irradiation. Thus the results obtained show that newly designed and synthesized compounds **PQSQ 1** and **PQSQ 2** have good photostability than reference dyes which may be attributed to a large pi-conjugated system and presence of additional terminal acceptors which decreases the electron density of pi-conjugated system [48]. In

Table 4
Computed photophysical parameters for **ISQ**, **N-Et ISQ**, **PQSQ 1** and **PQSQ 2** dyes in chloroform.

Compound	E_{HOMO} (eV)	E_{LUMO} (eV)	E_g[a] (eV)	VEE[b] (eV)	λ_{max}[c] (nm)	f[d]	Orbital contribution[e]
ISQ	−4.84	−2.49	2.35	2.21	560.67	1.7388	HOMO-LUMO (98.3)
N-Et ISQ	−4.89	−2.53	2.36	2.25	551.21	1.7470	HOMO-LUMO (98.3)
PQSQ 1	−4.72	−2.49	2.23	2.07	600.39	1.9324	HOMO-LUMO (97.6)
PQSQ 2	−4.81	−2.56	2.25	2.10	589.19	1.9353	HOMO-LUMO (97.4)

[a] HOMO-LUMO energy band gap.
[b] Computed vertical excitation energies.
[c] Computed absorption wavelength.
[d] Computed oscillator strength.
[e] Major electronic transition.

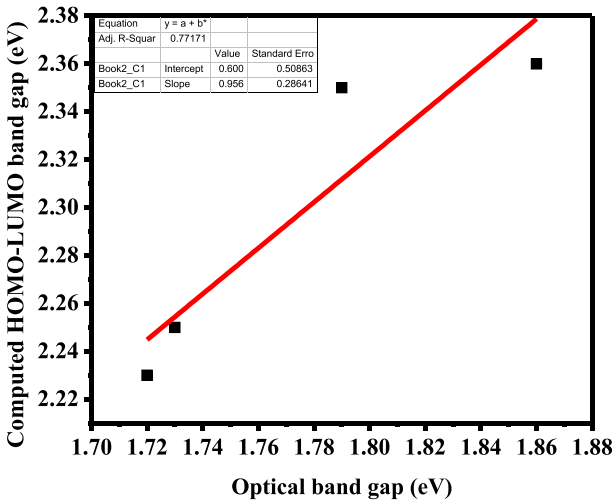

Fig. 14. Correlation of computed HOMO-LUMO band gap with optical band gap.

other words, the introduction of an additional acceptor on the D-A-D backbone enhances the photostability i.e. the dye with A^2-D-A^1-D-A^2 perform improved photostability compared with D-A-D type dyes.

3.7. Thermal Properties

To investigate the thermal stability of squaraines **PQSQ 1** and **PQSQ 2**, thermogravimetric analysis (TGA) was carried out within temperature range 30–600 °C under nitrogen gas at a heating rate of 10 °C min^{-1} (Fig. 12).

TGA thermogram of these dyes showed that they have good thermal stability with no remarkable weight loss at low temperature. The compound **PQSQ 1** has onset thermal decomposition temperature (T_d) of 327 °C with 5% weight loss. **PQSQ 2** however, is less stable than **PQSQ 1** and showed onset decomposition temperature at 246 °C. The thermogravimetric curves showed that the thermo-degradation pattern is influenced by alkyl groups. Thus compound having ethyl group, **PQSQ 2** showed less thermal stability compared to **PQSQ 1** which might be due to the presence of ethyl groups that weakens intermolecular van der walls and hydrogen bonding forces and decomposed first in presence of oxygen [49]. The high decomposition temperatures of these dyes indicated that they have quite stable thermal behavior.

4. Conclusion

In summary, we have designed and synthesized two novel NIR absorbing A^2-D-A^1-D-A^2 type symmetrical squaraines **PQSQ 1** and **PQSQ 2**, based on 2, 3, 3, 8-tetramethyl pyrrolo [3,2-h] quinoline to achieve absorption in NIR region and their photophysical properties were investigated. By utilizing terminal pyridyl acceptor groups on main D-A-D backbone, these dyes showed a bathochromic shift in absorption (33–44 nm) as well as emission (38–59 nm) compared to their parent indolenine based squaraines. Moreover, the negative solvatochromic behavior of these dyes was quantitatively evaluated by using ET (30) empirical solvent polarity parameter. The electrochemical properties of these dyes were also investigated and the novel squaraines exhibited irreversible electrochemical behavior. Additionally, the synthesized squaraines exhibited high thermal and photostability compared to their parent dyes. Density functional theory (DFT) was used to correlate structural parameters and photophysical properties of these compounds and results revealed that contribution of pyridine acceptor in LUMO orbital of compounds resulting in red-shifted absorption. We believe that the 2, 3, 3, 8-tetramethyl pyrrolo [3, 2-h] quinoline intermediate can be used to synthesize other classes of squaraine dyes such as symmetrical squaraines, unsymmetrical squaraines, thio squaraines, acceptor substituted squaraines for various properties and applications.

Acknowledgment

Authors are thankful to UGC-CAS for financial grant.

Appendix A. Supplementary data

Supplementary data to this article can be found online at https://doi.org/10.1016/j.saa.2018.11.061.

References

[1] G.M. Shivashimpi, S.S. Pandey, R. Watanabe, N. Fujikawa, Y. Ogomi, Y. Yamaguchi, Tetrahedron Lett. 53 (2012) 5437–5440.
[2] M. Büschel, A. Ajayaghosh, E. Arunkumar, J. Daub, Org. Lett. 5 (2003) 2975–2978.
[3] P.F. Santos, L.V. Reis, P. Almeida, A.S. Oliveira, L.F.V. Ferreira, J. Photochem. Photobiol. A Chem. 160 (2003) 159–161.
[4] S.H. Kim, S.H. Hwang, N.K. Kim, J.W. Kim, C.M. Yoon, S.R. Keum, Color. Technol. 116 (2000) 126–131.
[5] T. Inoue, S.S. Pandey, N. Fujikawa, Y. Yamaguchi, S. Hayase, J. Photochem. Photobiol. A Chem. 213 (2010) 23–29.
[6] P.F. Santos, L.V. Reis, P. Almeida, J.P. Serrano, S. Oliveira, L.F. Vieira Ferreira, J. Photochem. Photobiol. A Chem. 163 (2004) 267–269.
[7] S.H. Hwang, N.K. Kim, K.N. Koh, S.H. Kim, Dyes Pigments 39 (1998) 359–369.
[8] Y. Chandrasekaran, G.K. Dutta, R.B. Kanth, S. Patil, Dyes Pigments 83 (2009) 162–167.
[9] D.E. Lynch, M.Z.H. Chowdhury, N.L. Luu, E.S. Wane, J. Heptinstall, M.J. Cox, Dyes Pigments 96 (2013) 116–124.
[10] T. Maeda, Y. Hamamura, K. Miyanaga, N. Shima, S. Yagi, Org. Lett. (2011) 2009–2012.
[11] Y. Wang, S.Y. Gwon, S.H. Kim, Fibers Polym. 12 (2011) 836–838.
[12] D.D.S. Pisoni, C.L. Petzhold, M.P. Abreu, F.S. Rodembusch, L.F. Campo, C. R. Chim. 15 (2012) 454–462.
[13] L. Reis, J. Serrano, P. Almeida, P. Santos, Dyes Pigments 81 (2009) 197–202.
[14] I.V. Kurdiukova, A.V. Kulinich, A. Ishchenko, New J. Chem. 36 (2012) 1564–1567.
[15] S. Kuster, T. Geiger, Dyes Pigments 95 (2012) 657–670.
[16] S.H. Kim, S.H. Hwang, Dyes Pigments 35 (1997) 111–121.
[17] D.L. Ross, E. Reissner, J. Org. Chem. 31 (1966) 2571–2580.
[18] W. Yan, Q. Zhang, Q. Qin, S. Ye, Y. Lin, Z. Liu, Dyes Pigments 121 (2015) 99–108.
[19] Q. Tao, L. Duan, W. Xiong, G. Huang, P. Wang, H. Tan, Dyes Pigments 133 (2016) 153–160.
[20] G.D. Sharma, K.R. Patel, M.S. Roy, R. Misra, Org. Electron. Phys. Mater. Appl. 15 (2014) 1780–1790.
[21] L. Tong, P. Bi-Xian, F. Lou-Zhen, L. Yong-Fang, B. Feng-Lian, P. Zheng-Hong, Dyes Pigments 42 (1999) 113–116.
[22] A. Connell, P.J. Holliman, M.L. Davies, C.D. Gwenin, S. Weiss, M.B. Pitak, J. Mater. Chem. A 2 (2014) 4055–4066.
[23] S. Kim, G.K. Mor, M. Paulose, O.K. Varghese, C. Baik, C. Grimes, Langmuir 26 (2010) 13486–13492.
[24] T. Maeda, S. Arikawa, H. Nakao, S. Yagi, H. Nakazumi, New J. Chem. 37 (2013) 701–708.
[25] S. Yagi, T. Ohta, N. Akagi, H. Nakazumi, Dye Pigment 77 (2008) 525–536.
[26] S.H. Kim, S.K. Han, J.J. Kim, S.H. Hwang, C.M. Yoon, S.R. Keum, Dye Pigment 39 (1998) 77–87.
[27] U. Mayerhöffer, M. Gsänger, M. Stolte, B. Fimmel, F. Würthner, Chemistry 19 (2013) 218–232.
[28] M. Cheng, K. Aitola, C. Chen, F. Zhang, P. Liu, K. Sveinbjörnsson, Nano Energy 30 (2016) 387–397.
[29] R. Misra, R. Maragani, D. Arora, A. Sharma, G.D. Sharma, Dyes Pigments 126 (2016) 38–45.
[30] K. Mahesh, V. Priyanka, A.S. Vijai Anand, S. Karpagam, J. Mol. Struct. 1154 (2018) 445–454.
[31] H.S. Kumbhar, B.L. Gadilohar, G.S. Shankarling, Sensors Actuators B Chem. 222 (2016) 35–42.
[32] S.H. Kim, S.H. Hwang, Dyes Pigments 36 (1998) 139–148.
[33] W. Li, L. Li, H. Xiao, R. Qi, Y. Huang, Z. Xie, RSC Adv. 3 (2013) 13417–13421.
[34] J. Park, C. Barolo, F. Sauvage, N. Barbero, C. Benzi, P. Quagliotto, Chem. Commun. 48 (2012) 2782–2784.
[35] P. Marks, M. Levine, J. Chem. Educ. 89 (2012) 1186–1189.
[36] S. Miltsov, C. Encinas, J. Alonso, Tetrahedron Lett. 40 (1999) 4067–4068.
[37] F.S. Shakerizadeh, B. Hemmateenejad, A.M. Mehranpour, Anal. Methods 5 (2013) 891–896.
[38] S. Cha, M.G. Choi, H.R. Jeon, S.K. Chang, Sensors Actuators B Chem. 157 (2011) 14–18.
[39] L. Liu, J. Chen, Z. Ku, X. Li, H. Han, Dye Pigment 106 (2014) 128–135.
[40] Y. Ohsedo, M. Miyamoto, A. Tanaka, H. Watanabe, Dyes Pigments 101 (2014) 261–269.
[41] A.J. Bard, L.R. Faulkner, Electrochemical Methods: Fundamentals and Applications, 2nd Ed John Wiley & Sons, Inc., 2001 (chapter 6).
[42] A.D. Becke, J. Chem. Phys. 98 (1993) 5648–5653.
[43] F. Weigend, R. Ahlrichs, Phys. Chem. Phys. 7 (2005) 3297–3305.
[44] A. Duşa, J. Bus. Res. 60 (2007) 576–586.
[45] B. Camino, M.D.L. Pierre, A.M. Ferrari, J. Mol. Struct. 1046 (2013) 116–123.
[46] R.M. El-shishtawy, S.A. Elroby, A.M. Asiri, K. Müllen, Int. J. Mol. Sci. 17 (4) (2016) 487.
[47] X. Chen, X. Peng, A. Cui, B. Wang, L. Wang, R. Zhang, J. Photochem. Photobiol. A Chem. 181 (2006) 79–85.
[48] B. Song, Q. Zhang, W.H. Ma, X.J. Peng, X.M. Fu, B.S. Wang, Dyes Pigments 82 (2009) 396–400.
[49] M.R. Bhosle, L.D. Khillare, S.T. Dhumal, R.A. Mane, Chin. Chem. Lett. 27 (2016) 370–374.